THE ASTROPHYSICAL JOURNAL, 492:246–262, 1998 January 1

THE LOCATIONS OF GAMMA-RAY BURSTS MEASURED BY COMPTEL

R. MARC KIPPEN,[1,2,3] JAMES M. RYAN,[1] ALANNA CONNORS,[1] DIETER H. HARTMANN,[4]
CHRISTOPH WINKLER,[5] LUCIEN KUIPER,[6] MARTIN VARENDORFF,[7]
MARK L. MCCONNELL,[1] KEVIN HURLEY,[8] WIM HERMSEN,[6]
AND VOLKER SCHÖNFELDER[7]

Received 1997 May 29; accepted 1997 August 11

ABSTRACT

The COMPTEL instrument on the *Compton Gamma Ray Observatory* is used to measure the locations of gamma-ray bursts through direct imaging of MeV photons. In a comprehensive search, we have detected and localized 29 bursts observed between 1991 April 19 and 1995 May 31. The average location accuracy of these events is $1\overset{\circ}{.}25$ (1 σ), including a systematic error of $\sim 0\overset{\circ}{.}5$, which is verified through comparison with Interplanetary Network (IPN) timing annuli. The combination of COMPTEL and IPN measurements results in locations for 26 of the bursts with an average "error box" area of only ~ 0.3 deg^2 (1 σ). We find that the angular distribution of COMPTEL burst locations is consistent with large-scale isotropy and that there is no statistically significant evidence of small-angle autocorrelations. We conclude that there is no compelling evidence for burst repetition since no more than two of the events (or $\sim 7\%$ of the 29 bursts) could possibly have come from the same source. We also find that there is no significant correlation between the burst locations and either Abell clusters of galaxies or radio-quiet quasars. Agreement between individual COMPTEL locations and IPN annuli places a lower limit of ~ 100 AU (95% confidence) on the distance to the stronger bursts.

Subject headings: gamma rays: bursts — gamma rays: observations — methods: numerical — methods: statistical

1. INTRODUCTION

Cosmic gamma-ray bursts (GRBs) are among the brightest, most plentiful astrophysical phenomena in the observable gamma-ray sky, yet they present unique observational challenges. The greatest challenge is in measuring burst locations accurately. Because of this difficulty, much of our current understanding has come from large-scale statistical measures, where the accuracy of individual burst locations is not as important as the total number of bursts. The Burst and Transient Source Experiment (BATSE) has now measured the locations (accurate to $\sim 5°$, on average) and intensities of more than 1700 GRBs—yielding evidence that the sources are highly isotropic on the sky, yet radially inhomogeneous (e.g., Meegan et al. 1992; Briggs et al. 1996; Pendleton et al. 1996). These results rule out the once-favored galactic neutron star paradigm (e.g., Hurley 1986; Higdon & Lingenfelter 1990), but still allow three vastly different distance regimes: heliocentric (distance $D \lesssim 10^4$ AU), extended Galactic halo ($D \gtrsim 200$ kpc) and cosmological ($D \sim 1$ Gpc). The GRB mystery is thus far from being solved, as the range of possible distances spans over 12 orders of magnitude and the source objects remain elusive. In this paper we use the COMPTEL instrument aboard the *Compton Gamma Ray Observatory* (*CGRO*) to measure GRB locations with improved accuracy. A smaller sample of more accurate burst locations cannot improve upon large-scale measures, but improved location accuracy is a fundamental requirement for important studies of small-scale angular clustering, correlation with known objects, and searches for counterpart objects at other wavelengths. The large-scale distribution of unique subpopulations could also provide important insights.

Recent investigation of small-scale angular clustering of GRB sources has been hampered by the relative inaccuracy of locations measured with BATSE. Several statistical studies have yielded conflicting results, indicating both the presence (Quashnock & Lamb 1993; Wang & Lingenfelter 1993) and absence (Meegan et al. 1995; Brainerd et al. 1995; Tegmark et al. 1996) of small-angle correlations among BATSE burst locations. The presence of small-scale angular correlations would be important, as it could indicate repeating GRB sources or unresolved clusters, both of which are difficult to explain in most scenarios involving catastrophic destruction or mergers (e.g., Mészáros & Rees 1992; Narayan, Paczyński, & Piran 1992; White 1993; Katz 1993; Bickert & Greiner 1993). Earlier studies found no evidence to indicate burst repetition on timescales shorter than ~ 10 yr, but a majority of the locations used in these studies were also relatively inaccurate (Schaefer & Cline 1985; Atteia et al. 1987).

The investigation of cross-correlations between GRBs and catalogs of known objects has also been limited by imprecise locations. Most studies have failed to reveal a significant correlation with any Galactic or extragalactic source catalog (Howard et al. 1993; Nemiroff, Marani, & Cebral 1994, Harrison, Webber, & McNamara 1995). Recently, however, BATSE 3B burst locations have been

[1] Space Science Center, University of New Hampshire, Durham, NH 03824.
[2] Now at Center for Space Plasma and Aeronomic Research, University of Alabama, Huntsville, AL 35899.
[3] Mailing address: ES-84, NASA/Marshall Space Flight Center, Huntsville, AL 35812; marc.kippen@msfc.nasa.gov.
[4] Department of Physics and Astronomy, Clemson University, Clemson, SC 29634.
[5] Astrophysics Division, ESA/ESTEC, NL-2200 AG Noordwijk, The Netherlands.
[6] SRON-Utrecht, Sorbonnelaan 2, NL-3584 Utrecht, The Netherlands.
[7] Max-Planck-Institut für extraterrestrische Physik, Postfach 1603, D-85740 Garching, Germany.
[8] Space Sciences Laboratory, University of California, Berkeley, CA 94720.

reported to be weakly correlated ($\sim$2–3 σ significance) with galaxy clusters (Kolatt & Piran 1996; Marani et al. 1997; but see Hurley et al. 1997) and radio-quiet quasars (Schartel, Andernach, & Greiner 1997). Such correlations might be expected at some level if GRBs lie at cosmological distances characteristic of the galaxy samples, where the brighter, closer bursts are expected to show the strongest signal. However, no significant correlations with either galaxy clusters or quasars were found in an earlier analysis of accurate locations of bright GRBs, where one might expect a stronger signal (Webber et al. 1995).

Accurate burst locations are needed most importantly for the identification of counterpart objects at other wavelengths—a potential key to solving the GRB mystery. Unfortunately, quiescent counterpart emission at any wavelength appears to be very weak or nonexistent (see Vrba 1996). The last remaining hope is to detect transient counterpart emission soon after the onset in gamma rays—a particularly difficult challenge, as this requires quick and accurate GRB location. Most simultaneous and near-simultaneous measurements that have been obtained are relatively insensitive, but they indicate that if low-energy (i.e., non–gamma-ray) counterpart emission exists at all, it must be weak and/or short-lived ($<$1 day). Accurate and timely GRB localization is thus crucial for future counterpart search efforts (see McNamara, Harrison, & Williams 1995). The recent discovery of weak X-ray/optical emission from the directions of GRB 970228 and GRB 970508 offers the most convincing evidence obtained so far that GRBs do produce transient emission at other wavelengths (Costa et al. 1997a, 1997b; van Paradijs et al. 1997; Bond 1997). If these bursts are typical, then other counterparts will be detected only through the use of sensitive instruments combined with rapidly determined, accurate GRB locations.

The COMPTEL instrument has the unique capability of directly imaging MeV photon sources over a wide ($\sim$1 sr, FWHM) field of view (FoV). It is thus able to measure the locations and energy spectra of several GRBs per year. Full-sky exposure to bursts is achieved through long observations, over several years, during which the *CGRO* satellite is regularly repointed. In this paper we use the MeV imaging capability and effective full-sky coverage of COMPTEL to accumulate a comprehensive catalog of GRB locations observed during the first four years of the *CGRO* mission. This catalog constitutes a unique sample of relatively accurate locations that are used to investigate the GRB spatial distribution, providing insight into the distance/source object mystery. The energy spectra and temporal properties of these events have been discussed elsewhere (Kippen et al. 1996a, 1997 and references therein), as have preliminary locations of some of the bursts (see Table 1).

TABLE 1

COMPTEL Gamma-Ray Burst Location Catalog

Burst Name	BATSE Burst Trigger			$\hat{\lambda}$	ϑ_c	φ_c	α_{2000}	δ_{2000}	l	b	$\sigma_{\rm eff}$[b]	References for Preliminary Results
	No.	TJD	Seconds	(deg)	(deg)	(deg)	(deg)	(deg)	(deg)	(deg)	(deg)	
GRB 910425	109	8371	2265.7	40	44.4	266.2	90.2	−22.2	228.1	−20.6	0.92	1, 3, 5, 7, 17, 22, 23, 24, 25
GRB 910503	143	8379	25452.7	174	23.5	124.9	87.0	+38.6	172.0	+5.4	0.44	1, 2, 3, 4, 7, 17, 22, 23, 24, 25
GRB 910601	249	8408	69734.5	218	8.0	69.5	309.9	+32.7	74.1	−5.4	0.46	1, 3, 5, 7, 17, 22, 23, 24, 25
GRB 910627	451	8434	16157.8	22	10.8	223.0	199.4	−5.0	315.1	+57.3	1.63	3, 5, 7, 17, 22, 23, 24, 25
GRB 910709	503	8446	41602.1	36	37.5	32.5	144.1	+75.6	136.3	+36.0	1.80	17, 22, 23, 24, 25
GRB 910814	678	8482	69273.0	191	29.5	85.6	343.8	+29.5	94.7	−26.9	0.39	1, 3, 5, 7, 17, 22, 23, 24, 25
GRB 911118	1085	8578	68258.0	42	36.7	253.3	166.3	−22.5	273.0	+34.2	1.11	6, 7, 17, 22, 23, 24, 25
GRB 920622	1663	8795	25504.5	194	46.0	238.7	162.5	+49.2	161.3	+57.9	0.81	6, 18, 20, 22, 23, 24, 25
GRB 920627	1676	8800	46956.1	32	28.7	61.7	166.8	−8.5	263.9	+46.4	1.18	...
GRB 920830	1883	8864	6317.6	36	16.6	352.7	259.0	−74.5	318.0	−20.1	1.35	8, 18, 22, 23, 24, 25
GRB 930118[a].....	2137	9005	64427.0	21	15.7	21.9	221.8	−34.8	328.4	+22.3	1.47	8, 18, 22, 23, 24, 25
GRB 930131	2151	9018	68231.7	33	27.9	231.1	186.2	−7.9	291.6	+54.4	1.77	8, 9, 10, 15, 16, 18, 22, 23, 24, 25
GRB 930309	2228	9055	11269.8	43	29.9	100.2	322.7	+55.2	96.9	+2.8	0.74	8, 11, 15, 18, 22, 23, 24, 25
GRB 930612	2387	9150	2657.7	23	24.1	83.4	106.5	−71.0	282.0	−24.4	1.60	22, 23, 24, 25
GRB 930704	2428	9172	60545.7	22	19.2	79.5	99.3	+62.8	152.5	+22.4	1.08	12, 19, 22, 23, 24, 25
GRB 931229	2715	9350	26165.9	32	49.2	314.3	241.9	+21.0	36.2	+45.1	2.35	22, 23, 24, 25
GRB 940217	2831	9400	82962.1	367	10.4	307.2	30.1	+3.1	154.5	−55.5	0.32	13, 21, 22, 23, 24, 25
GRB 940301	2855	9412	72637.1	149	8.0	254.6	102.7	+64.0	151.6	+24.1	0.40	12, 14, 19, 22, 23, 24, 25
GRB 940314	2881	9425	35989.1	34	14.5	48.8	356.0	−1.4	88.0	−59.6	1.43	25
GRB 940520	2984	9492	1298.7	56	23.4	219.6	324.7	+7.7	62.5	−31.8	0.70	25
GRB 940619	3035	9522	77480.6	28	27.5	108.4	298.5	−31.5	9.3	−26.3	1.15	25
GRB 940708	3067	9541	74526.2	69	5.6	134.8	300.5	+22.7	61.1	−4.2	1.03	25
GRB 940728	3101	9561	86334.1	21	14.9	27.6	85.1	−38.0	243.2	−29.6	1.10	25
GRB 940921	3178	9616	18493.1	138	30.8	1.2	207.1	−16.4	322.3	+44.4	0.68	25
GRB 941017	3245	9642	37173.0	68	62.2	258.9	301.7	+13.3	53.7	−10.0	2.10	25
GRB 950208	3408	9756	7824.0	40	37.6	123.6	344.8	+56.0	107.6	−3.5	1.95	25
GRB 950421	3516	9828	44989.6	36	15.3	0.2	70.1	−61.7	272.1	−39.0	1.43	25
GRB 950425	3523	9832	919.2	337	47.6	171.9	164.9	−33.8	277.8	+23.6	0.34	25
GRB 950522	3593	9859	85283.2	100	36.2	72.0	110.8	+20.3	197.9	+15.9	1.14	...

[a] This burst was detected by BATSE during the data readout period following a solar flare.

[b] Angular radius of a circle having the same area as the irregularly shaped COMPTEL 1 σ confidence region.

References.—(1) Schönfelder et al. 1991; (2) Winkler et al. 1992a; (3) Varendorff et al. 1992; (4) Winkler et al. 1992b; (5) Connors et al. 1993a; (6) Connors et al. 1993b; (7) Winkler et al. 1993; (8) Varendorff et al. 1993; (9) Kippen et al. 1993a; (10) Ryan, Kippen, & Varendorff 1993; (11) Bennett et al. 1993; (12) Ryan et al. 1994a; (13) Kippen et al. 1994a; (14) Kippen et al. 1994b; (15) Kippen et al. 1994c; (16) Ryan et al. 1994b; (17) Hanlon et al. 1994; (18) Kippen et al. 1995a; (19) Kippen et al. 1995b; (20) Greiner et al. 1995; (21) Winkler et al. 1995; (22) Kippen et al. 1995c; (23) Kippen et al. 1995d; (24) Kippen et al. 1995e; (25) Kippen et al. 1996b.

2. INSTRUMENTATION AND FUNDAMENTAL ANALYSIS

2.1. *Instrument Characteristics*

COMPTEL is a wide-field, double-scatter Compton telescope capable of imaging gamma-ray sources in the energy range 0.75–30 MeV. It consists of two planar layers of scintillation detector modules separated by ~ 1.5 m. The upper (D1) layer incorporates seven low-Z, low-density liquid (NE213A) detectors (total area 4188 cm^2), while the lower (D2) layer is composed of 14 high-Z, high-density NaI(Tl) modules (total area 8620 cm^2). A *telescope event* is defined as a coincident set of interactions in a single pair of (D1, D2) modules in anticoincidence with a signal from any of four plastic charged particle veto domes. For each telescope event, the energy deposits and interaction locations within each detector are measured using the signals from photomultiplier tubes affixed to the detector modules. The interaction sequence from D1 to D2 is identified by a time-of-flight (ToF) coincidence measurement, and the absolute time of each event is tagged with an accuracy of 125 μs. Rejection of a large fraction of neutron-induced background events is realized through the measurement and discrimination of pulse shape (PSD) in D1.

The COMPTEL design favors the ideal interaction in which an incident photon undergoes a single Compton scatter in D1, followed by complete absorption of the scattered photon in D2. For such ideal telescope events, the measurement of energy deposits in D1 and D2 yields the scattered electron energy and scattered photon energy, respectively, while the measurement of interaction locations within the detectors reveals the direction of the scattered photon. Combined, the energy and location information constrains the incident photon direction to an annular ring or *event circle* on the sky. The angular radius $\bar{\varphi}$ of an event circle is determined by the kinematics of Compton scattering:

$$\cos \bar{\varphi} = 1 - m_e c^2 \left(\frac{1}{E_2} - \frac{1}{E_1 + E_2} \right), \qquad (1)$$

where $m_e c^2$ is the electron rest energy and E_1 and E_2 are the energy deposit measurements in D1 and D2, respectively. Ambiguity about the arrival direction of individual photons is removed through the statistical superposition of many events with different scatter angles, thereby forming a unique source signature. Complicating matters are nonideal source events, such as those arising from multiple Compton scatters, pair production in D1, or incomplete energy absorption in the detectors, for which equation (1) is invalid. Nonideal events result in a complicated source signature that must be accounted for in the imaging analysis. Selection criteria applied to event parameters (i.e., E_1, E_2, $\bar{\varphi}$, ToF, and PSD) during analysis can significantly alter the effective energy range, sensitivity, and FoV of the instrument. A complete description of COMPTEL and its operation and performance has been presented by Schönfelder et al. (1993).

2.2. *Burst Detection Capabilities*

COMPTEL employs two independent operating modes for observing transient phenomena such as gamma-ray bursts. In parallel with the main *telescope mode*, a secondary *burst mode* uses two of the D2 modules to accumulate time-resolved spectra in the energy range 0.1–10 MeV (see Hanlon et al. 1994 and references therein). In this paper, we are concerned only with the source localization capabilities of the telescope mode observations.

In detecting and localizing gamma-ray bursts, COMPTEL is in most cases a photon-limited device, the sensitivity of which is governed by low detection efficiency rather than by background. Sensitivity in this case depends on burst fluence, with the minimum detectable fluence given by

$$S_{\min} = \frac{\bar{E} N_S}{A_{\text{eff}}}, \qquad (2)$$

where $\bar{E}$ is the spectrum-dependent mean photon energy (0.75–30 MeV), A_{eff} is the effective detection area for ideal events, and N_S is the number of ideal source events that are required to construct a meaningful image (Winkler et al. 1986). Requiring 20 ideal events from a normally incident E^{-2} power-law burst source ($A_{\text{eff}} = 31$ cm^2; $\bar{E} = 2.8$ MeV) yields $S_{\min} = 4.5 \times 10^{-6}$ erg cm^{-2}. Burst sensitivity decreases as the zenith angle ϑ_c between the telescope pointing axis and the source direction increases. This relation effectively limits the FoV for bursts to $\vartheta_c \lesssim 60°$. This is illustrated in Figure 1*a* for several different power-law energy spectra. The strong dependence of burst sensitivity on fluence (rather than, e.g., peak flux) results in a significant bias against the detection of short-duration bursts, since short bursts typically do not result in enough events for meaningful imaging (even though the instantaneous flux may be large).

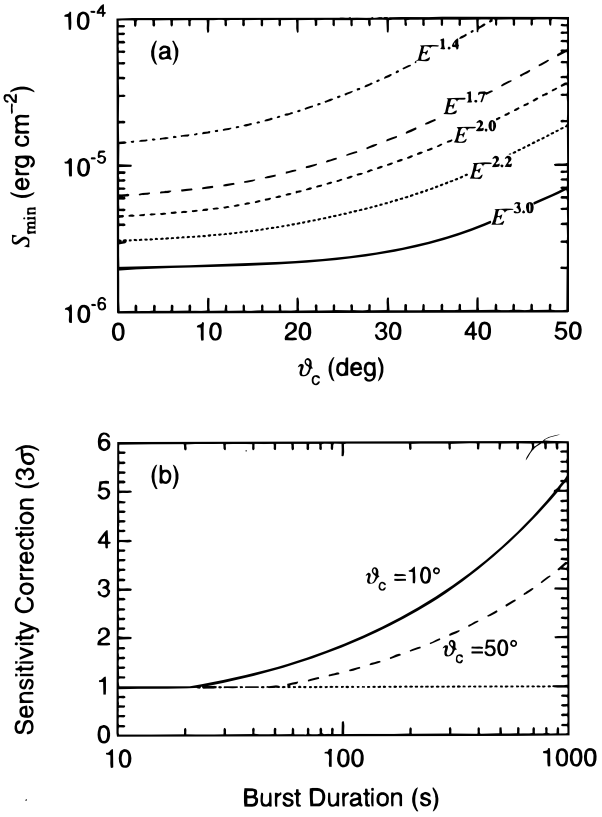

FIG. 1.—The estimated sensitivity of COMPTEL to gamma-ray bursts. (*a*) The minimum detectable fluence $S_{\min}$ (0.75–30 MeV) as a function of burst viewing angle ϑ_c for several different power-law energy spectra, assuming zero background. For bursts longer than ~ 25 s, the estimates in (*a*) must be multiplied by a background correction factor (*b*), which also depends on the viewing angle and can change by a factor of ~ 3 as a result of orbital variations.

The average rate of background events that could be confused with ideal source events ranges from ~ 0.2 Hz at $\vartheta_c = 50°$ to ~ 0.6 Hz at $\vartheta_c = 10°$, with orbital variations as large as a factor of 3. Background is thus significant only in the detection of longer duration, low-fluence bursts. The statistical detection significance for such bursts is

$$\sigma_{\rm det} \approx \frac{N'_S}{\sqrt{N'_S + 2N_B}}, \tag{3}$$

where N'_S is the number of source counts (related to the burst fluence through eq. [2]), and N_B is the number of background counts (roughly proportional to burst duration). When the number of source counts required for a significant detection above background (N'_S) exceeds the number of counts required for imaging ($N_S \sim 20$), detection is background-limited. In this case, the sensitivity estimates of Figure 1*a* are too low. Correction factors (roughly independent of spectral shape) for $\sigma_{\rm det} = 3$ are plotted as a function of burst duration in Figure 1*b*. The detection of bursts shorter than ~ 25 s is effectively always photon-limited regardless of zenith angle. For longer bursts, background becomes increasingly important. Fortunately, most long-duration bursts contain short, intense episodes, the detection of which is less dependent on background.

For very intense bursts, or burst intervals, where fluence $S \gtrsim 10^{-4}$ erg cm^{-2}, electronics and telemetry deadtime limit the ability of COMPTEL to register and record events. This affects the detection of short, intense bursts, where significant numbers of events fail to be registered and/or recorded. Deadtime thus produces an additional bias against the detection of short-duration bursts.

2.3. *Burst Imaging Analysis*

The imaging analysis of COMPTEL data is performed in a three-dimensional dataspace defined by the quantities $(\chi, \psi, \bar{\varphi})$. The coordinates (χ, ψ) define the direction of the vector between the (D1, D2) interaction locations and the scatter angle $\bar{\varphi}$ is computed from the energy deposit measurements using equation (1). In this representation, the point source signature, or point spread function (PSF), is a partially filled cone with a 45° opening angle whose vertex is centered on the source position (Fig. 2). The complicated diagonal shape of the cone mantle is determined by the inherent measurement errors and the physics of nonideal interactions, all functions of source position and energy spectrum. Dependence of the PSF shape on source position is weakened by factoring out a geometry term $\mathcal{G}$ (see Schönfelder et al. 1993). This allows (to some degree of approximation) the use of a single PSF for imaging sources located anywhere in the FoV. The PSF used for all burst source analyses in this paper has been derived from a Monte Carlo simulation (see Stacy et al. 1996) of the COMPTEL response to a point source of gamma rays at $\vartheta_c = 10°$ with an assumed E^{-2} power-law energy spectrum. Various standard selections are imposed on the event data in order to reduce systematic effects arising from incomplete knowledge of the PSF and to improve the signal-to-noise ratio in the data (see Schönfelder et al. 1993). These selections are applied equally to the PSF simulations and to the data.

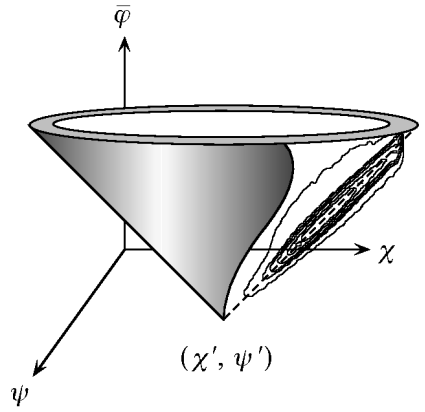

FIG. 2.—Illustration of the three-dimensional COMPTEL response to a point source located at sky coordinates (χ', ψ'). Contours show a cross section of the response function indicating the off-diagonal effects of intrinsic measurement errors and nonideal interactions.

The imaging process amounts to searching for the PSF signature in the binned $(\chi, \psi, \bar{\varphi})$ distribution of telescope events (a mixture of source and background). The bin size is chosen to be on the order of the instrumental resolution (1°, 1°, and 2° in χ, ψ, and $\bar{\varphi}$, respectively), resulting in a few events per bin. A maximum likelihood search technique capable of handling the sparsely populated dataspace is employed to obtain quantitative constraints on the source parameters. The maximum likelihood method, described fully by de Boer et al. (1992), attempts to fit a point source (PSF) plus a model of the background signature to the three-dimensional dataspace distribution of events, assuming Poisson counting statistics. For a trial source position, the likelihood of source plus background $\mathcal{L}(\mathrm{S+B})$ and the likelihood of the null hypothesis of pure background $\mathcal{L}(\mathrm{B})$ are independently maximized by allowing PSF and background scale factors (but not shape) to vary. A sky map of the quantity

$$\lambda = 2 \ln \left[\frac{\mathcal{L}(\mathrm{S+B})}{\mathcal{L}(\mathrm{B})} \right], \tag{4}$$

the maximum likelihood ratio, or MLR, is used to estimate and constrain the source location and the statistical significance of detection. The most probable source position corresponds to the maximum $\lambda \equiv \hat{\lambda}$ in the sky map, which *formally* obeys the χ^2 probability distribution with 3 degrees of freedom (source intensity and position). Thus, $\hat{\lambda} \gtrsim 14.2$ indicates a statistically significant 3 σ detection. For such significant detections, the source location is constrained by the quantity $\Delta\lambda = \hat{\lambda} - \lambda$, which is distributed as χ^2_2 so that formal 1 σ, 2 σ, and 3 σ statistical confidence regions in the sky map are defined where $\Delta\lambda \lesssim 2.3$, 6.2, and 11.8, respectively.

The formal relation between likelihood ratio and χ^2 is based on the implicit assumption of an accurate PSF and background model. The form of the background model is thus an important part of burst imaging, even though the number of background events during bursts is typically small. The dataspace distribution of background events present during GRBs is difficult to model owing to complicated temporal and spatial variations. An empirical model provides the most practical means of approximation, but background count rates are too low to provide a sufficient statistical sample of the full three-dimensional distribution. Fortunately, the (χ, ψ) component of this distribution is reasonably approximated by the geometry function $\mathcal{G}$ mentioned above. The $\bar{\varphi}$ component embodies much of the

background complexity. It is determined independently for each burst by directly sampling events that were detected under orbital history conditions similar to the burst observation. In practice, this is done by sampling events within a window of satellite orbital parameters chosen to approximate the orbital history of *CGRO* at the time of a burst, and thereby the background environment during the burst. The $\bar{\varphi}$ distribution of directly sampled background events is combined with the geometry function (properly normalized) to form a three-dimensional background model that is then used in the imaging process. An example of real and modeled background is shown in Figure 3.

2.4. *Systematic Imaging Errors*

The approximations used in the imaging process are all potential sources of systematic errors in the derived burst source parameters (i.e., source significance and localization). The major sources of error are: 1) the use of a single PSF for all bursts, regardless of source location or energy spectrum, 2) statistical fluctuations in the PSF, 3) the inherent accuracy of Monte Carlo simulations used to compute the PSF, and 4) the accuracy of the background model. The effects of each of these approximations have been studied with the use of simulations similar to those used to determine the PSF. Unfortunately, since all combinations of potential causes of error cannot possibly be simulated, this technique serves only as a predictive estimate of the true errors.

Simulated sources with various, burst-like energy spectra, distributed throughout the FoV and mixed with samples of real background were subjected to the full imaging process with a variety of PSFs. The distribution of offsets between known source parameters and those derived through imaging analysis of the simulated bursts yields an estimate of systematic errors. We find that the use of a single PSF for all bursts has the largest effect on source location accuracy, especially for $\vartheta_c \gtrsim 30°$, but that the error is never more than 0°.75. The other potential causes of location error contribute only minimally. Overall, simulated sources are correctly localized by the MLR imaging technique to within an error of 0°.5 ($\sim$90% confidence). We also find that $\hat{\lambda}$ (indicating detection significance) is correctly determined to within an error of approximately $\sim$30%. The largest contributing cause of error in this case is the background model, since the shape of the background in the observed COMPTEL dataspace is difficult to model accurately. The largest errors in $\hat{\lambda}$ are for sources located near the earth's limb, where atmospheric gamma rays contribute most to the background and are not approximated well by our model. Bursts located near the earth's limb also result in source photons backscattering off the atmosphere, which confuses the true source signature.

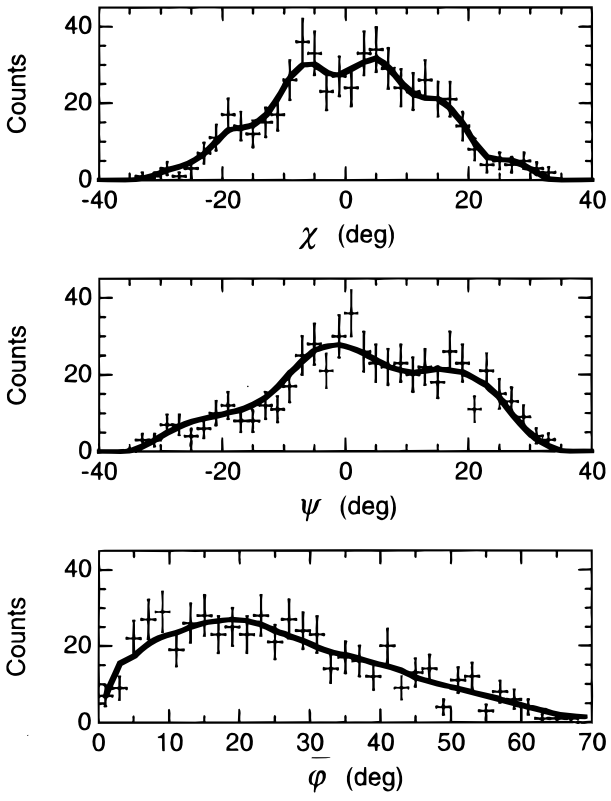

FIG. 3.—An example of the spatial distribution of COMPTEL background events during a gamma-ray burst. Observed (*data points*) and modeled (*solid lines*) distributions are shown summed along each of the three dataspace coordinates.

3. OBSERVATIONS

3.1. *Burst Search Strategy*

To identify potential COMPTEL gamma-ray bursts, we rely on the BATSE transient event triggering system. This system automatically detects statistically significant count rate (50–300 keV) increases above background in the BATSE large-area detectors (Fishman et al. 1989). Triggers can be from gamma-ray bursts, solar flares, magnetospheric activity, Earth occultation of strong celestial sources, or terrestrial atmospheric events. The COMPTEL burst search strategy is to examine data only from the times of BATSE triggers that are classified as GRBs by the BATSE analysis team (Mallozzi et al. 1993) and whose BATSE locations satisfy $\vartheta_c < 65°$. This strategy is effective in identifying COMPTEL GRB candidates. An exception occurs during BATSE data accumulation and readout periods following all triggers (Meegan et al. 1996). The BATSE trigger system is disabled during these accumulation periods (usually lasting either 4 or 8 minutes) and is insensitive to new, weaker events during data readout intervals (usually 90 minutes). These gaps in coverage must be taken into account when computing the exposure to bursts, as explained in § 4.1.

In the period between 1991 April 19 and 1995 May 31 there were 3608 BATSE triggers, 1297 of which have been classified as GRBs. Of these, 397 have BATSE locations with $\vartheta_c < 65°$. COMPTEL data are available for only 302 of the 397 burst candidates because of gaps in telemetry caused by the failure of *CGRO* data recorders in 1992. Data from around the time of each candidate trigger ($\pm$15 minutes) have been manually examined to identify potential burst intervals. Time intervals showing the most evidence for significant counts above background were subjected to the maximum likelihood imaging process. In cases where time intervals of significant emission were ambiguous, the approximate full duration of the burst as measured by BATSE was used for imaging. MLR maps were computed over a grid of sky coordinates with $1° \times 1°$ spacing, and a final burst detection threshold was applied to the images by requiring $\hat{\lambda} > 20$—formally indicating a 3.8 σ point source detection. The possibility of systematic error in the determination of $\hat{\lambda}$ is accounted for by using a conservative detec-

tion threshold. This ensures that only significant excesses ($\gtrsim 3\ \sigma$) are accepted. We expect, at the most, one spurious detection in the search of 302 candidates.

3.2. *COMPTEL Gamma-Ray Burst Location Catalog*

Over the four years of observations, we have accumulated a catalog of 29 gamma-ray bursts that satisfy the $\hat{\lambda} > 20$ detection requirement. These bursts are summarized in Table 1. Each detection is identified by the year (*yy*), month (*mm*) and day (*dd*) of the burst in the form GRB *yymmdd*. The next three columns give the number, truncated Julian day (TJD), and seconds of the day of the corresponding BATSE burst trigger. This is followed by the value of $\hat{\lambda}$ and the most probable COMPTEL burst location expressed in Spacecraft (ϑ_c, φ_c), Celestial (α, δ; epoch J2000.0) and Galactic (l, b) coordinates. Preliminary locations of many of the bursts have been published earlier, as indicated. This catalog includes two bursts in addition to those reported in the preliminary analysis of Kippen et al. (1996b). One of these bursts (GRB 920627) was mistakenly neglected in the preliminary search and the other (GRB 950522) was beyond the time interval of the earlier analysis.

Statistical uncertainty regions around the most probable burst locations have been estimated by computing smoothed (cubic spline) contours of the MLR sky maps corresponding to 1 σ, 2 σ, and 3 σ confidence levels. Celestial coordinate sky maps of these contours are shown in Figure 4. In general, the localizations are irregularly shaped regions, making it difficult to compare uncertainties between different bursts. A convenient *approximate* measure of the statistical location error is given by the radius of a circle having the same area as the region enclosed by the MLR contours. The value of this quantity ($\sigma_{\rm eff}$) for the 1 σ confidence level is given in Table 1. The statistical location error is usually inversely related to the number of source events. Thus, the error radius of a high-fluence burst such as GRB 940217 ($\sigma_{\rm eff} = 0.^\circ32$) is much smaller than that of a weaker detection such as GRB 910627 ($\sigma_{\rm eff} = 1.^\circ63$). This behavior is complicated, however, by the character of the off-axis telescope response, which introduces additional uncertainty in the azimuthal (φ_c) direction for all bursts at large zenith angle ($\vartheta_c \gtrsim 30^\circ$). The average statistical location uncertainty, as approximated by $\sigma_{\rm eff}$, for the full COMPTEL burst sample is $1.^\circ13$. A circle with this angular radius is included in each of the plots in Figure 4 for comparison. Note that systematic errors are not included in the MLR localizations.

3.3. *Measured Systematic Burst Location Error*

As indicated in the sky maps of Figure 4, 26 of the 29 COMPTEL bursts have been independently localized through the method of arrival time analysis using the *CGRO* and *Ulysses* spacecraft as two nodes of an Interplanetary Network (IPN) baseline (Hurley et al. 1992). This technique constrains the direction of a burst to a thin annulus on the sky centered at coordinates ($l_{\rm arc}$, $b_{\rm arc}$), with typical angular radius $R_{\rm arc} \sim 50^\circ$ and width $\sigma_r \lesssim 0.^\circ1$ (Hurley et al. 1996). The perpendicular offset ρ between the most probable COMPTEL burst location (l, b) and the corresponding IPN annulus is given by

$$\rho = \cos^{-1}\left[\sin b \sin b_{\rm arc} + \cos b \cos b_{\rm arc} \cos (l - l_{\rm arc})\right] - R_{\rm arc}\ , \quad (5)$$

where positive and negative values indicate whether the COMPTEL location is inside or outside the annulus, respectively. This quantity provides a convenient measure of the total COMPTEL location error (statistical and systematic) in one dimension. We have used the *CGRO*/*Ulysses* IPN annuli of 26 bursts to directly estimate the average COMPTEL systematic burst location error (cf. Graziani & Lamb 1996).

We began by simulating many COMPTEL "catalogs" of burst positions, with each position randomly blurred according to the statistical error distributions described by the MLR maps. An additional systematic blurring error was applied to the positions in the form of a symmetric Gaussian probability function with a 68% confidence radius, $\sigma_{\rm sys}$. For each random burst position, the quantity $\rho_{\rm sim}$ was determined from equation (5), assuming that the corresponding IPN annulus passed directly through the centroid of the input (for the simulation) burst position. Uncertainty in the IPN annulus width was incorporated by assuming a Gaussian error distribution with standard deviation σ_r. Using the Kolmogorov-Smirnov test, we computed the maximum deviation of the cumulative distribution of observed ρ from that obtained with 2000 blurred catalogs ($\rho_{\rm sim}$). By varying $\sigma_{\rm sys}$ and repeating the procedure, we determined how large $\sigma_{\rm sys}$ must be in order to minimize the deviation between the observed and blurred distributions. We found that $\sigma_{\rm sys} = 0.^\circ6 \pm 0.^\circ4$ yields the best fit within a 68% confidence interval. The observed and best-fit differential distributions of ρ are shown in Figure 5. This measurement is entirely consistent with the value of $\sigma_{\rm sys} = 0.^\circ5$ discussed above, estimated by independent means. For all subsequent analysis, we took $\sigma_{\rm sys} = 0.^\circ5$ and assumed that this was constant for all bursts. When this error is added in quadrature to the statistical error radius ($\sigma_{\rm eff}$), the average COMPTEL location uncertainty increases to $1.^\circ25$.

3.4. *Combined COMPTEL/IPN Localizations*

The COMPTEL burst localizations are reduced over an order of magnitude in area by incorporating the constraints provided by IPN measurements. The COMPTEL localizations were used to limit the probable extent of the IPN annuli in the following manner. First, the probability distributions obtained from the observed MLR maps were convolved with a Gaussian systematic blurring function with $\sigma_{\rm sys} = 0.^\circ5$. This provided, for each burst, a measure of the total COMPTEL location error distribution around the most likely position. The convolved maps were then evaluated at $0.^\circ1$ intervals along the corresponding IPN annuli, yielding probability as a function of angular distance along the annuli. The most probable combined COMPTEL/IPN location of a burst corresponds to the point of maximum probability along the arc, and confidence intervals were obtained from the integral probability distribution. Uncertainty in the width of the combined locations was assumed to be dominated by IPN measurement errors that are small compared to COMPTEL errors.

Combined COMPTEL/IPN burst localizations are listed in Table 2, where the most probable combined locations are expressed in Celestial (epoch J2000.0) and Galactic coordinates. The next column gives the mean 68% confidence error σ_a in the angular distance along the arc, as measured from the most probable position. This is followed by the uncertainty in the arc width σ_r, as determined from IPN timing measurements (Hurley et al. 1996). Those bursts that

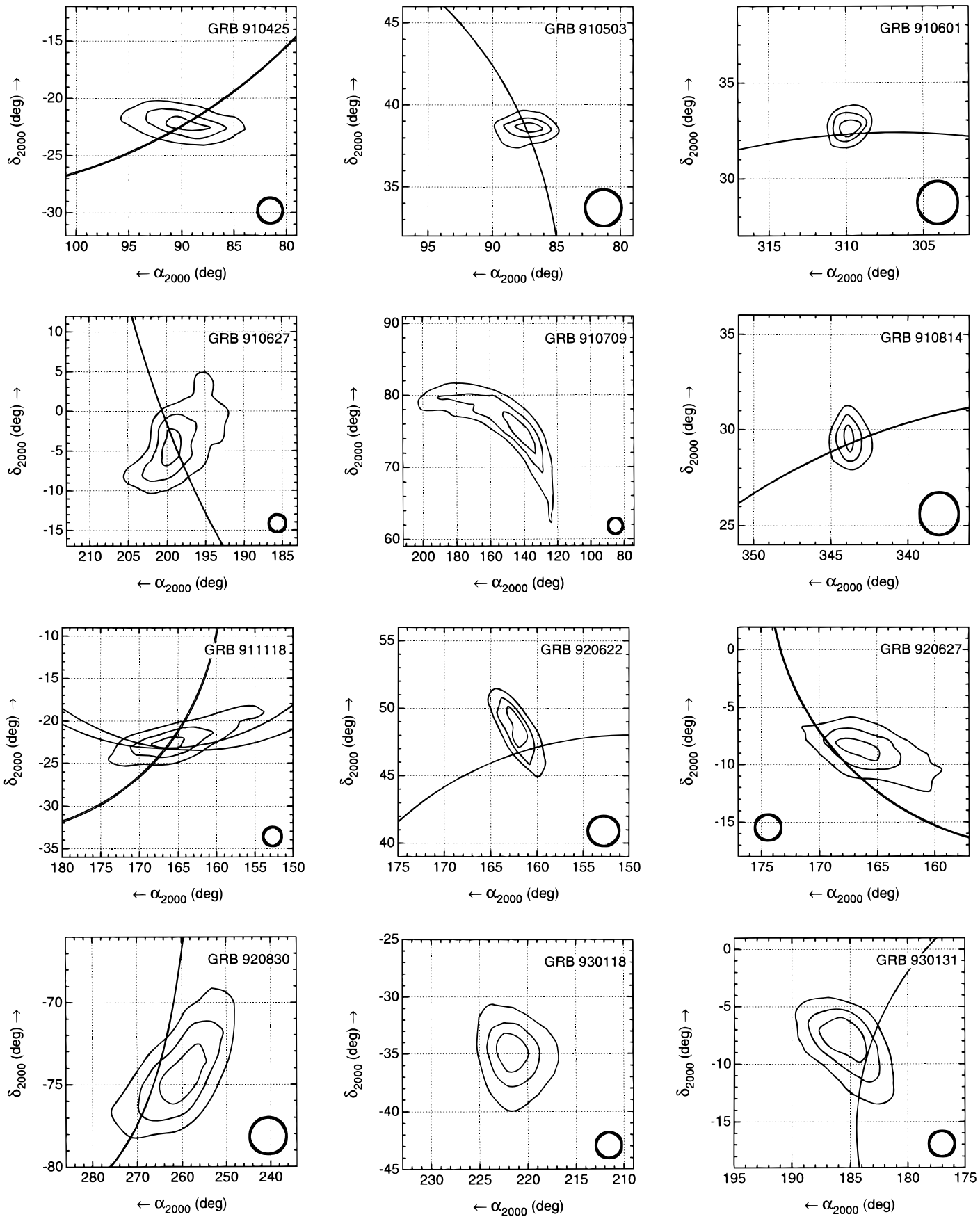

FIG. 4.—These plots show the locations of each of the COMPTEL bursts in Celestial coordinates (epoch J2000.0). Smoothed contours obtained through maximum-likelihood imaging enclose 1 σ, 2 σ, and 3 σ statistical confidence regions. Where available, IPN timing annuli (Hurley et al. 1996) are overlaid, with the 3 σ error in the annulus width indicated by two concentric arcs. For scale reference, a circle corresponding to the average 1 σ area of all the bursts (angular radius 1°.13) is shown in each plot (*thick line*).

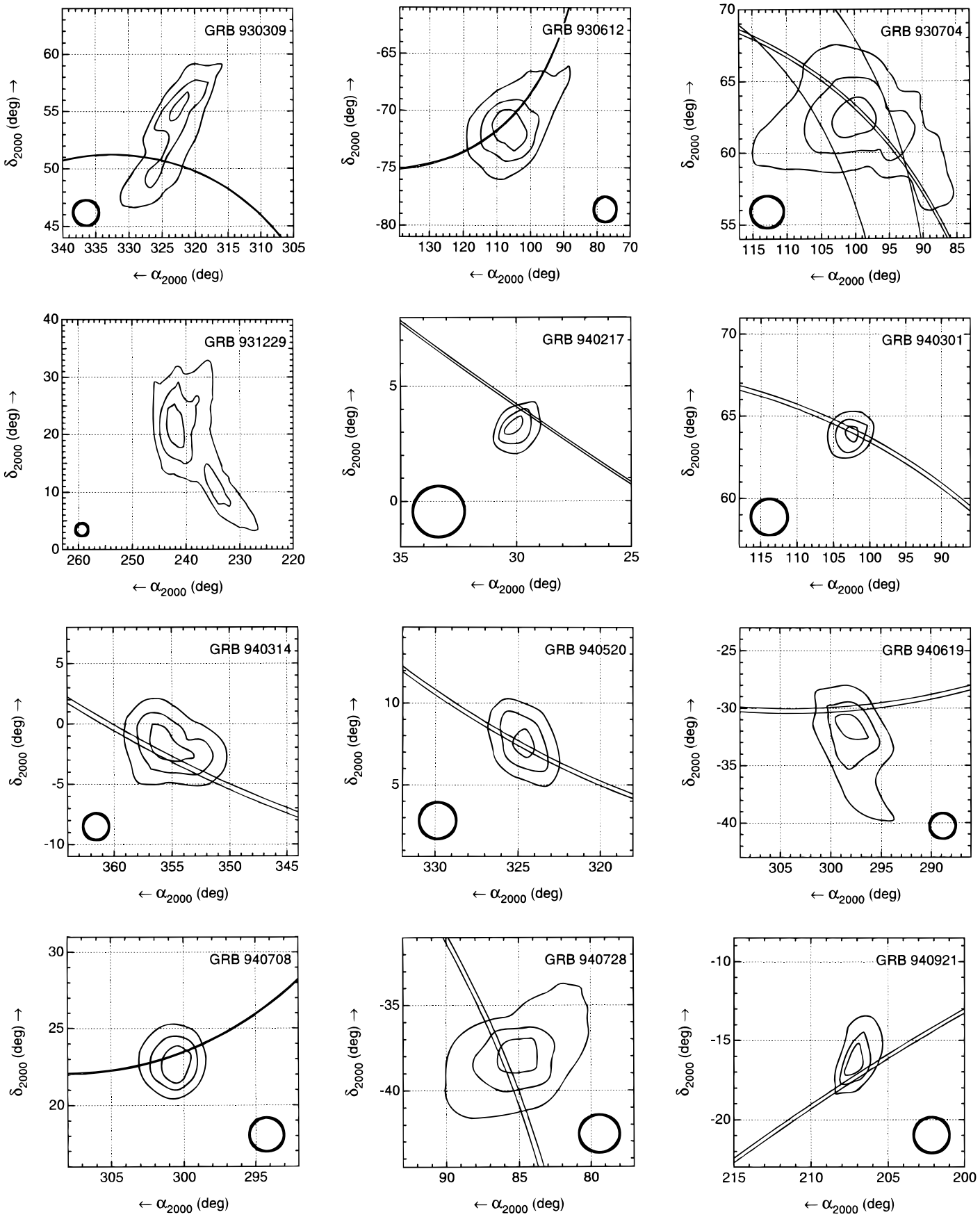

FIG. 4—*Continued*

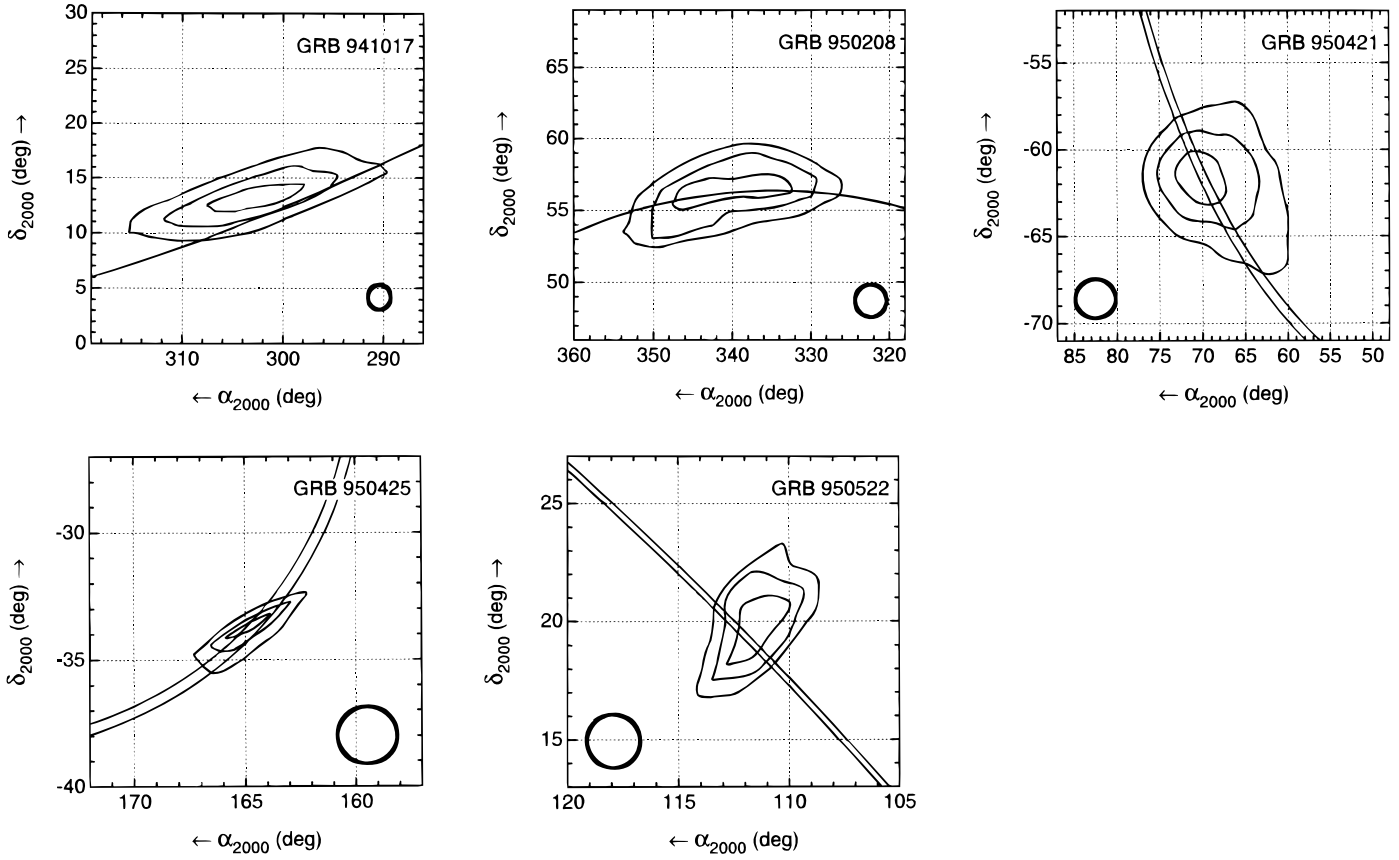

FIG. 4—*Continued*

were observed by more than two spacecraft are indicated. The average COMPTEL/IPN burst localization (1 σ confidence) corresponds to a short, thin arc segment with total length $2 \times \langle \sigma_a \rangle = 1.^\circ 97$ and total width $2 \times \langle \sigma_r \rangle = 0.^\circ 13$. For one burst (GRB 911118), IPN measurements from three spacecraft provide a nearly unambiguous determination of the source location at which the individual annuli intersect. The IPN location of this event is within the COMPTEL statistical 1 σ MLR contour (see Fig. 4).

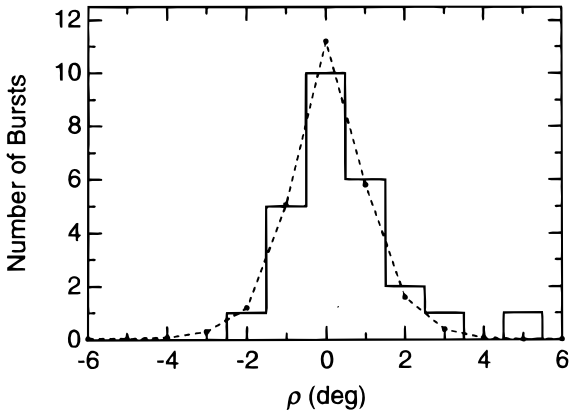

FIG. 5.—Distribution of the angle ρ between most likely COMPTEL burst positions and IPN annuli (at closest approach) for 26 bursts. The solid histogram shows the measured distribution, while the dashed curve is the best-fit model incorporating statistical COMPTEL and IPN errors and a constant COMPTEL systematic location error of $0.^\circ 5$.

4. SPATIAL DISTRIBUTION ANALYSIS

Despite their limited number, the COMPTEL GRB catalog locations provide a useful measure of the global angular distribution of GRBs. In principle, the catalog can also be used to probe the GRB distance scale through the distribution of burst intensities (e.g., Pendleton et al. 1996; Fenimore et al. 1993). However, the COMPTEL measurements are ill suited to this purpose because of severe observational biases, most notably the strong dependence of burst sensitivity on fluence (and duration), the large variation of sensitivity across the FoV, and the inability to measure intense burst episodes because of deadtime. These biases would require large, uncertain correction factors at nearly all observed intensity levels. The COMPTEL locations can, however, shed some light on the burst distance dilemma through correlations with known objects and by providing a lower limit on the distance to individual events through comparison with IPN measurements.

We analyzed the distribution of COMPTEL burst locations using two inclusive samples chosen for easy comparison with results of earlier analyses. The 3 yr sample includes 18 bursts observed between 1991 April 19 and 1994 March 1, while the 4 yr sample incorporates the full catalog of 29 bursts. Galactic coordinate distributions of the COMPTEL statistical location constraints for both burst samples are shown in Figure 6. The null hypothesis is that GRB sources have an isotropic angular distribution on all size scales, with no preferred direction or clustering. We use the COMPTEL bursts as a sample of the full GRB population to test this hypothesis. The small number of bursts means

TABLE 2

COMPTEL/IPN Gamma-Ray Burst Locations[a]

Burst Name	α_{2000} (deg)	δ_{2000} (deg)	l (deg)	b (deg)	σ_a (deg)	σ_r (deg)	Spacecraft[b]
GRB 910425.....	89.78	−22.30	227.99	−21.03	0.56	0.053	C, U
GRB 910503.....	87.43	+38.62	172.13	+5.73	0.29	0.010	C, U
GRB 910601.....	309.92	+32.33	73.82	−5.67	0.36	0.011	C, U
GRB 910627.....	198.63	−4.35	313.91	+58.04	1.43	0.031	C, U
	198.83	−4.52	314.23	+57.84	1.35	0.036	U, P
GRB 910709.....	...	...	...	...	...	...	...
GRB 910814.....	343.78	+29.31	94.54	−27.09	0.35	0.018	C, U
	343.78	+29.32	94.54	−27.08	0.37	0.019	U, P
GRB 911118.....	166.16	−23.21	273.30	+33.46	1.98	0.017	C, U
	166.48	−23.23	273.62	+33.59	1.78	0.019	U, P
	166.06	−22.59	272.84	+33.96	0.61	0.086	P, C
GRB 920622.....	161.42	+46.86	165.83	+58.44	0.35	0.009	C, U
GRB 920627.....	169.04	−8.36	266.57	+47.69	1.14	0.049	C, U
GRB 920830.....	266.05	−74.67	318.75	−21.82	1.08	0.018	C, U
GRB 930118.....	...	...	...	...	...	...	...
GRB 930131.....	183.65	−9.72	288.10	+52.10	0.97	0.003	C, U
GRB 930309.....	324.93	+50.72	94.90	−1.43	0.66	0.035	C, U
GRB 930612.....	106.88	−70.88	281.94	−24.21	0.98	0.053	C, U
	110.65	−69.97	281.34	−22.75	1.05	1.289	C, M
GRB 930704.....	99.46	+62.98	152.32	+22.48	1.53	0.113	C, U
	99.99	+62.40	153.00	+22.55	1.05	2.319	C, M
GRB 931229.....	...	...	...	...	...	...	...
GRB 940217.....	29.50	+3.83	152.97	−55.11	0.29	0.020	C, U
GRB 940301.....	102.01	+64.20	151.35	+23.88	0.37	0.090	C, U
GRB 940314.....	355.74	−2.56	86.35	−60.49	1.29	0.220	C, U
GRB 940520.....	324.71	+7.39	62.34	−32.05	0.66	0.059	C, U
GRB 940619.....	298.59	−30.05	10.81	−25.95	0.91	0.081	C, U
GRB 940708.....	300.59	+23.27	61.65	−3.98	0.64	0.038	C, U
GRB 940728.....	85.94	−38.38	243.80	−29.00	0.74	0.131	C, U
GRB 940921.....	207.01	−17.24	321.77	+43.56	0.55	0.121	C, U
GRB 941017.....	298.14	+13.09	51.68	−7.22	3.16	0.016	C, U
GRB 950208.....	344.78	+55.94	107.63	−3.57	2.95	0.022	C, U
GRB 950421.....	69.78	−61.77	272.19	−39.14	1.14	0.226	C, U
GRB 950425.....	164.69	−33.77	277.62	+23.52	0.66	0.207	C, U
GRB 950522.....	111.82	+19.22	199.32	+16.35	0.57	0.063	C, U

[a] IPN data from Hurley et al. (1996).

[b] IPN spacecraft: C = *Compton Gamma Ray Observatory* (BATSE), U = *Ulysses*, P = *Pioneer Venus Orbiter*, M = *Mars Observer*.

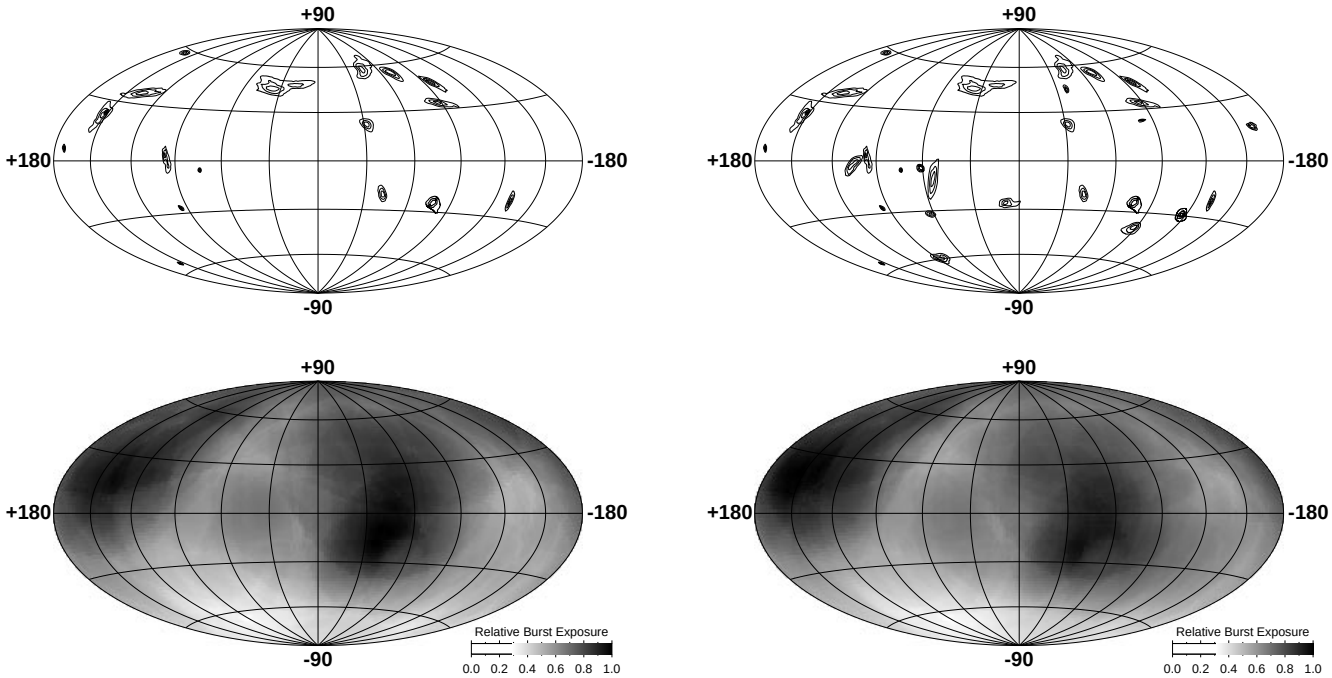

Fig. 6.—The COMPTEL statistical (1 σ, 2 σ, and 3 σ) location contours (*top*) and corresponding burst exposure functions (*bottom*), plotted in Galactic coordinates. The leftmost plots correspond to the 3 yr observation period (18 bursts), while the plots at right include the full 4 yr interval (29 bursts).

that statistical fluctuations are the dominant source of error and that this error is non-Gaussian. Statistical tests are therefore conducted by Monte Carlo methods. The major observational biases present are the nonideal burst locations and uneven sampling of the sky, both of which affect the interpretation of the data.

4.1. *Burst Exposure Function*

The limited extent and varying sensitivity of the COMPTEL FoV, combined with *CGRO*'s low Earth orbit and sporadic pointing schedule, result in a complicated sampling pattern over the sky that modifies the intrinsic angular source distribution. We must determine this pattern—the *burst exposure function*—in order to correct the observational bias it produces.

Assuming that bursts occur isotropically in space and uniformly in time, the relative probability $P_{\rm exp}$ of detecting a burst from a particular direction in the sky as opposed to any other direction is given by

$$P_{\rm exp} = t_{\rm on} \times \int_{S_{\rm min}}^{\infty} \frac{dN}{dS}\, dS\ , \tag{6}$$

where $t_{\rm on}$ is the time spent observing the direction of interest, $S_{\rm min}$ is the minimum fluence for a detection, and dN/dS is the differential burst size–frequency distribution (i.e., the number of bursts per year with 0.75–30 MeV fluence between S and $S + dS$). Evaluation of $P_{\rm exp}$ is complicated by the function $S_{\rm min}$, which depends on the source position within the FoV, the background rate, and the burst energy spectrum. We approximated $P_{\rm exp}$ by ignoring background and taking the burst energy spectrum to be the average power law ($E^{-2.6}$; Kippen et al. 1996a, 1997), leaving $S_{\rm min}$ as a function only of sky position through equation (2). A further problem is that dN/dS is not well known in the COMPTEL energy range. For simplicity, we used a power law of the form $dN/dS \propto S^{-3/2}$. For strong bursts, such as those observed by COMPTEL, this is a reasonable approximation (Fenimore et al. 1993).

The above approximations were used to compute $P_{\rm exp}$ for every 16 s of observation on a grid of sky coordinates with $2^\circ \times 2^\circ$ spacing. Directions occulted by the earth were excluded, as were all epochs when COMPTEL and/or the BATSE trigger system were disabled or the spacecraft was not telemetering data. Directions outside the $\vartheta_c \leq 65^\circ$ search window were also excluded. Sky maps of the burst exposure function accumulated over the two analysis intervals are shown in Figure 6. The maximum value of $P_{\rm exp}$ in the 3 and 4 yr exposure maps is 426 and 624 effective days, respectively. In both maps, the minimum exposure is at least 30% of the maximum, meaning that all portions of sky have been observed at a reasonable level. The smooth fluctuations on top of this minimum exposure reflect the frequent Earth occultation of directions along the Celestial equator and the schedule of the *CGRO* pointing program. In particular, the south Galactic polar region received the least exposure, while a great deal of time was spent observing the Galactic plane and Virgo ($l = 270^\circ$, $b = 60^\circ$) regions. The effects of different spectral shapes, burst intensity function, and the inclusion or exclusion of BATSE data accumulation periods are small ($\lesssim 10\%$) compared to the overall magnitude of the structures in the exposure maps.

4.2. *Large-Scale Angular Distribution*

Studies of large-scale angular structure have been most concerned with the question of whether burst sources reside inside or outside our Galaxy. Two convenient and sensitive statistical tools for this particular purpose are the dipole and quadrupole moments in Galactic coordinates (e.g., Hartmann & Epstein 1989; Paczyński 1990; Briggs 1993). The dipole moment (expressed as $\langle \cos \Theta \rangle$, where Θ is the angle between a burst and the Galactic center) measures the concentration toward the center of the Galaxy, while the quadrupole moment (expressed as $\langle \sin^2 b - \frac{1}{3} \rangle$, where b is the Galactic latitude of a burst) indicates the concentration toward the Galactic plane. Significant nonzero values of the moments indicate deviations from an isotropic source distribution. Similar statistics, expressed in Celestial coordinates (i.e., $\langle \cos \Theta \rangle$, where Θ is the angle from the Celestial origin and $\langle \sin^2 \delta - \frac{1}{3} \rangle$, where δ is declination), are more sensitive to the biases caused by the nonuniform COMPTEL exposure function.

The dipole and quadrupole moments expected for an isotropic angular distribution of sources are modified by the nonuniform burst exposure function. The magnitude of this effect was estimated by simulating random catalogs of burst locations chosen according to the COMPTEL exposure function maps. An ensemble of moments computed from 5×10^4 simulated catalogs provides a measure of the exposure-induced deviation from isotropy and the statistical uncertainty inherent in the number of bursts in each catalog. The largest deviation from the isotropic value appears in the Celestial quadrupole moment, where the exposure function produces a 0.7 σ bias toward polar declinations (in both 3 and 4 yr samples). The exposure-induced bias in Galactic coordinates is much smaller (see examples in Fig. 7).

Observed moments were estimated by randomly blurring each of the measured burst locations according to the total (statistical and systematic) location error distributions. An ensemble of moments computed from many blurred catalogs provides a measure of the error induced by imprecise locations. As illustrated in Figure 7, this effect is small compared to the statistical uncertainty caused by the low number of bursts. The difference between the observed and expected moments yields the true or corrected deviation from isotropy. Corrected values of the dipole and quadrupole moments are given in Table 3 in both Galactic and celestial coordinates. Uncertainties in the corrected moments reflect 68% confidence limits on the difference between the data and the simulations. Within the sizable uncertainties, there are no significant deviations from large-scale isotropy evident in the COMPTEL burst samples in either Galactic or celestial coordinates.

4.3. *Small-Scale Angular Distribution*

The dipole and quadrupole moments are sensitive only on the largest of angular scales ($\theta \gtrsim 60^\circ$). Different statistical tests are necessary to investigate the small-scale angular distribution of burst sources. The two standard approaches are the angular autocorrelation function $w(\theta)$ and the nearest-neighbor function $nn(\theta)$. Both statistics are sensitive to small-scale angular structure on the order of the instrumental resolution, which might suggest either intrinsic source clustering or repeated bursts from individual sources. It has been shown that the angular correlation function provides superior sensitivity to small-scale angular structure when the number of sources is large, such that the average separation between neighboring positions is less

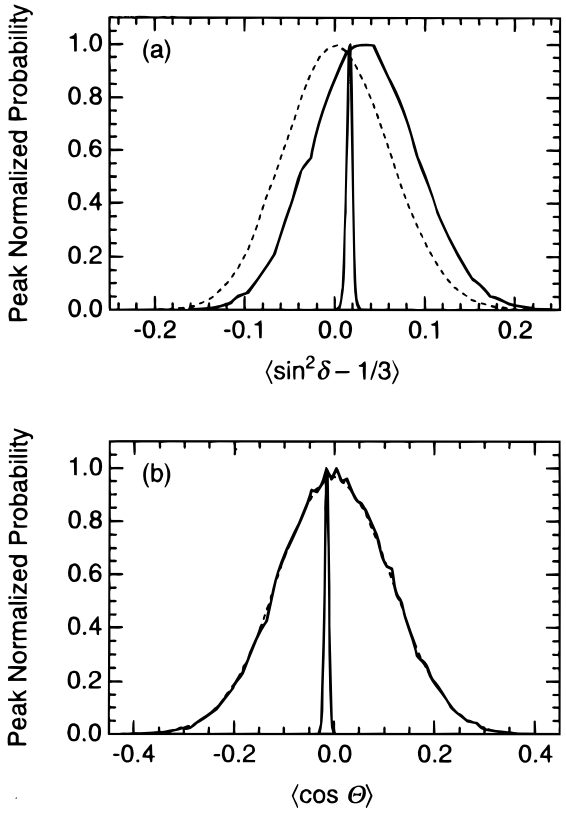

FIG. 7.—Simulations of (*a*) Celestial quadrupole moment and (*b*) Galactic dipole moment distributions for 29 burst locations. The narrowest distributions in each case represent the values observed by COMPTEL, including the effect of location errors. The remaining curves show the statistical distributions expected from isotropy assuming uniform (*dashed curves*) and nonuniform (*solid curves*) burst exposure functions.

than the average location accuracy (Brainerd 1996). This is not the case for the small sample of well-localized COMPTEL bursts, where the average neighbor separation ($\sim 20°$) is much greater than the average location accuracy ($\sim 1.°25$). Hence, both tests were used.

The angular correlation function, first applied to GRB positions by Hartmann & Blumenthal (1989) and Hartmann, Linder, & Blumenthal (1991), measures the probability of finding a pair of sources separated by an angle θ. It is computed by comparing the number of source pairs $N_{\rm obs}$ with angular separations in the range $(\theta, \theta + d\theta)$ to the number of pairs $N_{\rm exp}$ expected from a random sample of an isotropic distribution with

$$w(\theta) = \frac{N_{\rm obs}}{N_{\rm exp}} - 1 \, . \tag{7}$$

The presence of small-scale angular clustering is evident in $w(\theta)$ as a significant positive deviation from zero at small angles. The nearest-neighbor function $nn(\theta)$, first used on GRB positions by Quashnock & Lamb (1993), differs slightly in that it compares the number of sources with one or more neighbors separated by $(\theta, \theta + d\theta)$ to the number expected in a random, isotropic sample. Small-scale clustering is evident in $nn(\theta)$ as a significant excess above the expected value at small angles. Both statistics are affected by imprecise source locations, which spread the intrinsic signal of clustering over a range of θ characteristic of the average location accuracy. The signal of small-scale clustering is maximized by choosing bins in θ with the same characteristic size.

Figure 8 shows the angular correlation and nearest-neighbor distributions for the two samples of COMPTEL burst locations. Angular bins of 2° were used to approximate the average location accuracy at the 90% confidence level, where the signal from clustering would be most apparent. The distributions of $N_{\rm exp}$ expected from isotropy were determined by taking the average of 5×10^4 simulated catalogs, each chosen at random according to the corresponding burst exposure function. The effect of nonuniform exposure on the $N_{\rm exp}$ distributions is small compared to statistical fluctuations among the random catalogs ($< 0.1\ \sigma$). The statistical significance of observed deviations in excess of the isotropic expectation was estimated by the fraction of simulated catalogs Q with an equal or greater excess in the angular bin in question.

The most significant small-angle excess is evident in the first 2° bin in the 3 yr catalog distributions, where $Q = 4.8 \times 10^{-2}$. This excess occurs because two of the bursts (GRB 930704 and GRB 940301) are localized to the same direction within their combined location errors—something that is not expected in a random sample of only 18 sources (Ryan et al. 1994a). This near coincidence of two bursts occurring 8 months apart was investigated by Kippen et al. (1995b) and Hanlon et al. (1995), who computed a similar chance probability for the observation ($Q = 3.0 \times 10^{-2}$). The value of Q computed here is somewhat larger mainly because of the addition of the previously neglected burst GRB 920627. Kippen et al. (1995b) could neither prove nor rule out the possibility that the two bursts originated from a single source, even when all other avail-

TABLE 3

LARGE-SCALE ANGULAR DISTRIBUTION MEASURES

	3 yr SAMPLE		4 yr SAMPLE	
STATISTICAL TEST	Value	Deviation[a]	Value	Deviation[a]
Galactic:				
$\langle \cos \Theta \rangle$	-0.124 ± 0.140	-0.886	-0.016 ± 0.110	-0.145
$\langle \sin^2 b - \frac{1}{3} \rangle$	$+0.001 \pm 0.068$	$+0.015$	-0.023 ± 0.053	-0.434
Celestial:				
$\langle \cos \Theta \rangle$	-0.091 ± 0.129	-0.705	$+0.026 \pm 0.101$	$+0.257$
$\langle \sin^2 \delta - \frac{1}{3} \rangle$	$+0.034 \pm 0.073$	$+0.466$	-0.022 ± 0.057	-0.386

[a] Number of standard deviations of the measured value from isotropy.

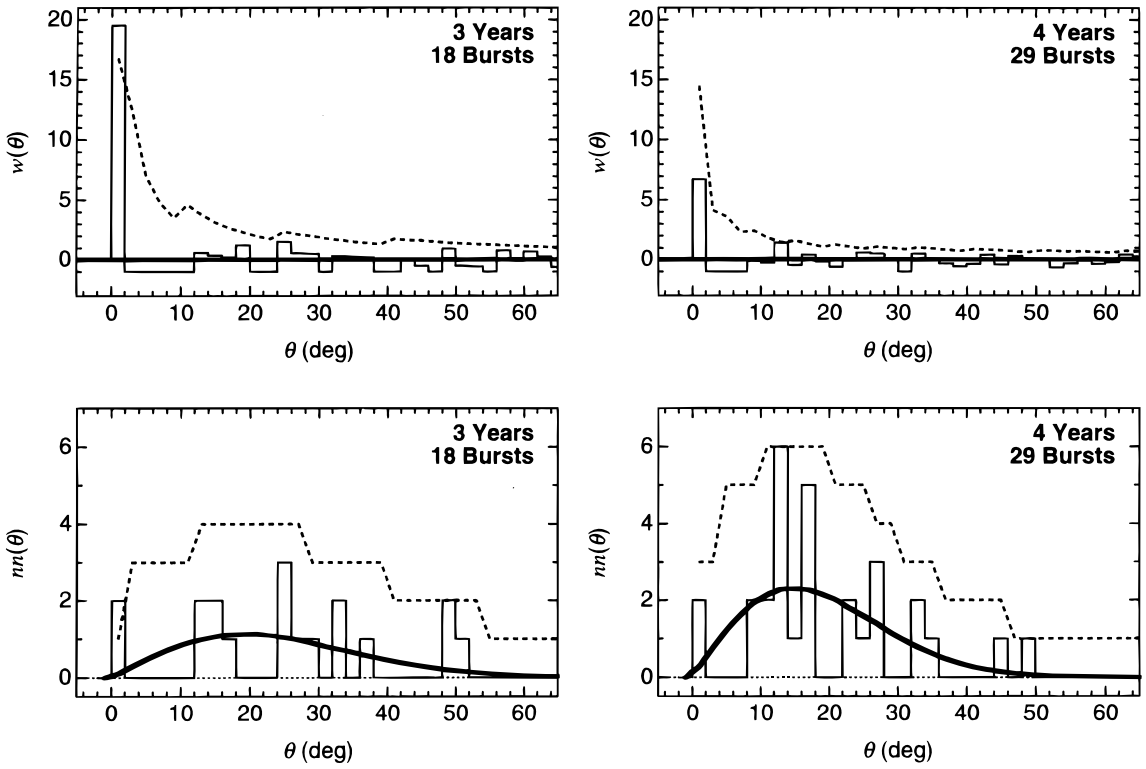

FIG. 8.—Angular autocorrelation functions $w(\theta)$ and nearest-neighbor distributions $nn(\theta)$ of two samples of COMPTEL burst locations. Each plot compares the distribution measured with the most likely locations (*solid histograms*) to the distributions expected from the nonuniform sampling of isotropy (*solid curves*). Dashed curves indicate the magnitude of statistical deviations from the expected distributions at the 90% significance level.

able measurements were included (IPN, BATSE, and *CGRO*-EGRET). In the larger 4 yr sample, the significance of the excess at $\theta < 2°$ is reduced to $Q = 1.2 \times 10^{-1}$, as a result of the fact that no additional bursts from the possible repeating source were observed in the year following GRB 940301, and no other coincident pairs were measured elsewhere. We therefore conclude that the 4 yr sample is consistent with isotropy on small scales.

4.4. *Correlation with Galaxy Catalogs*

Examination of correlations between GRBs and catalogs of known objects is similar to the study of self-clustering described above. Statistical tools such as the nearest-neighbor test and the angular correlation function are simply modified by computing angles between GRB/object pairs rather than angles between pairs of different bursts. As in the case of self-clustering, cross-correlations between GRBs and known objects are affected by burst location errors, which spread the cross-correlation signal over an angular range characteristic of the average burst location error. Although many different types of astronomical catalogs have been examined, we chose to concentrate only on galaxy clusters and radio-quiet quasars, which have been suggested to correlate with BATSE 3B burst locations (Kolatt & Piran 1996; Marani et al. 1997; Schartel, Andernach, & Greiner 1997). In particular, we used the galaxy cluster catalog of Abell, Corwin, & Olowin (1989, hereafter ACO), and the quasar catalog of Véron-Cetty & Véron (1996, hereafter VCV). The full ACO catalog (ACO-1) contains 5250 galaxy clusters, categorized by several parameters, including richness class R and distance class D. A subset of the 185 ACO galaxy clusters with $R \geq 1$ and $D \leq 4$ (ACO-2) was examined separately, since this particular subset had been suggested to show a correlation with the most accurate BATSE burst locations (Marani et al. 1997 and references therein). The VCV catalog contains 11,662 quasars and active galactic nuclei. We examined only the radio-quiet quasars, as selected by Schartel, et al. (1997). The full radio-quiet quasar sample (VCV-1) contains 7146 objects. A subset of 967 radio-quiet quasars with redshift $z \leq 1.0$ and absolute magnitude $M_{abs} \leq -24.2$ (VCV-2) was also examined, since this sample shows the strongest correlation with BATSE GRBs.

The computation of angular cross-correlation between COMPTEL GRBs and ACO/VCV catalog locations was performed, as in the case of self-clustering. In each 2° angular bin the number of observed GRB/catalog pairs, N_{obs}, was compared to the average number obtained from 5×10^4 random COMPTEL "catalogs," N_{exp}, (sampled from the 4 yr COMPTEL burst exposure function) using equation (7). Table 4 lists the results for GRB/catalog pair angular separations $\theta < 2°$. The uncertainty in N_{exp} given in the table reflects the standard deviation of the random catalogs, and Q is the statistical significance of the observed number of pairs compared to the expected number. None of

TABLE 4

GRB/GALAXY CORRELATION STATISTICS

Catalog	Objects	N_{obs}	N_{exp}	Q
ACO-1.....	5250	46	42.9 ± 12.0	0.390
ACO-2.....	185	3	1.6 ± 1.4	0.218
VCV-1.....	7146	25	53.8 ± 45.0	0.736
VCV-2.....	967	10	7.7 ± 5.7	0.286

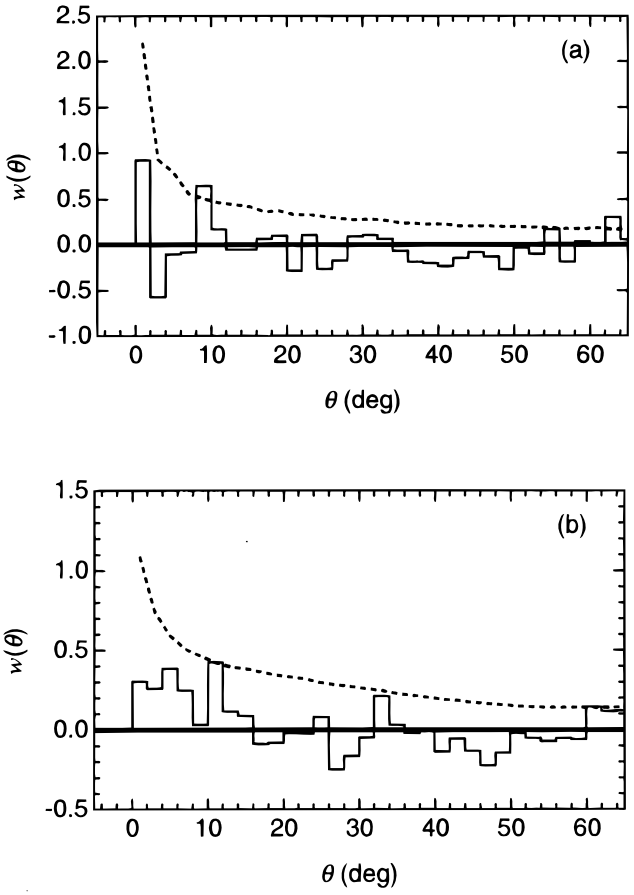

FIG. 9.—Angular cross-correlation function $w(\theta)$ between 29 COMPTEL burst locations and: (*a*) 185 ACO galaxy clusters with richness class $R \geq 1$ and distance class $D \leq 4$; (*b*) 967 VCV radio-quiet quasars with redshift $z \leq 1.0$ and absolute magnitude $M_{abs} \leq -24.2$. Each plot compares the distribution observed with the most likely COMPTEL burst locations (*solid histograms*) to the distribution expected, on average, from random samples of the nonuniform COMPTEL exposure function (*solid lines*). Dashed curves indicate the magnitude of statistical deviations from the expected distributions at the 90% significance level.

the four catalog samples show a significant correlation with COMPTEL GRB locations at small angles, where one would expect the signal if an association exists. Angular cross-correlation functions for the ACO-2 and VCV-2 object catalogs are shown in Figure 9.

4.5. *COMPTEL/IPN Burst Distance Limits*

While a "local" GRB source population has not been examined in as much detail as the more distant possibilities, such an origin (i.e., sources within 10^4 AU) is not inconsistent with the angular and intensity distributions observed by BATSE (Maoz 1993; Horack et al. 1994). Lower limits on the distances to burst sources are therefore important. As pointed out by Hurley (1982), timing differences between four or more widely separated IPN spacecraft in a favorable configuration could be used to yield a lower limit for the burst source distance. While only a few events have been observed by this many IPN spacecraft, the idea can also be applied to the bursts localized by COMPTEL and the *CGRO/Ulysses* IPN.

If a burst is observed by two spacecraft separated by a distance b, the angle α between the burst direction and the inter-spacecraft baseline is

$$\cos \alpha = \left(\frac{c\,\Delta t}{b}\right) + \frac{b}{2D}\left[1 - \left(\frac{c\,\Delta t}{b}\right)^2\right], \qquad (8)$$

where c is the speed of light, D is the distance to the burst source, and Δt is the observed difference in burst arrival times between the two spacecraft (Connors et al. 1993a). Thus, $\cos \alpha$ is larger than that inferred from the time delay alone ($\cos \alpha = \cos R_{arc} = c\,\Delta t/b$) by a parallax factor that is inversely related to the source distance. If the offset of a burst position from an IPN annulus were measured, it would reveal the source distance. The fact that COMPTEL burst localizations agree with IPN annuli to within the COMPTEL location accuracy places a lower limit on the distance to burst sources. The severity of this limit improves with the accuracy of the COMPTEL localization (in the direction perpendicular to the IPN annulus) and the length of the IPN baseline b.

According to the procedure described in § 3.4, the total (statistical and systematic) COMPTEL localization of a burst can be maximized along an annulus to reveal the most likely combined position and the probability at that position. In computing a quantitative COMPTEL/IPN distance limit, this technique was applied to a set of concentric annuli with angular radii α progressively smaller than R_{arc}. This yielded—through equation (8)—the COMPTEL location probability as a function of source distance D. Uncertainty in the width of the IPN annuli was incorporated by substituting $R_{arc} + \sigma_r$ in the calculation of probability as a function of D. Integration of this function at the desired confidence level yields a lower limit. The most constraining distance lower limits (D_{min}) at the 2 σ confidence level are listed in Table 5. Even when all known systematic location errors are conservatively included, the distance to these bursts must be at least $\sim$100 AU in order to be consistent with the COMPTEL/IPN measurements.

TABLE 5

COMPTEL/IPN GAMMA-RAY BURST DISTANCE LOWER LIMITS[a]

Burst Name	R_{arc} (deg)	σ_r (deg)	b (AU)	D_{min} (AU)
GRB 910601.....	52.936	0.011	3.708	109.4
GRB 920622.....	41.335	0.009	5.800	79.8
GRB 920830.....	86.268	0.018	6.271	180.3
GRB 940217.....	69.334	0.050	3.038	137.5
GRB 940921.....	54.361	0.121	2.583	90.1

[a] IPN data from Hurley et al. 1996.

5. SUMMARY AND DISCUSSION

We have demonstrated the ability of COMPTEL to accurately localize GRB sources through direct Compton scatter imaging. This ability has been used to accumulate a unique collection of locations for bursts having a high fluence of gamma rays in the energy range 0.75–30 MeV. Analysis of the COMPTEL locations has shown that these bursts, apparently like all others, are consistent with an isotropic angular distribution of sources. Furthermore, we find no statistically significant excess of GRB locations clustered at small angles, as would be expected if many of the sources we observed burst repeatedly on timescales of several months. We also find no significant cross-

correlation with ACO galaxy clusters or radio-quiet VCV quasars, and have placed a lower limit on the distance to GRB sources by comparing the COMPTEL locations to IPN timing annuli. The COMPTEL measurements thus contribute to our understanding of the GRB phenomenon in each of the three currently feasible source distance regimes.

For a local heliospheric origin, the distance constraints required by COMPTEL/IPN burst location measurements dispute any scenarios in which the sources of brighter (and therefore closer, assuming bursts are roughly "standard luminosity candles") GRBs are nearer than ~ 100 AU (approximately the distance of the solar wind termination shock). Relativistic dust grain models (Grindlay & Fazio 1974; Dasgupta 1979) and nearby (40–400 AU) colliding comet scenarios (White 1993, 1994) are therefore unlikely. More distant Oort cloud models involving mergers between comets, antimatter, and/or primordial black holes (Katz 1993; Dermer 1996; Bickert & Greiner 1993) are not excluded by our distance limits. However, dynamical simulations of potential Oort cloud GRB progenitor distributions indicate that it is difficult to restrict GRBs only to the outer, more distant portions of the cloud (Clarke, Blaes, & Tremaine 1994). In order to obey the angular and intensity distributions measured with BATSE *and* the distance lower limits reported here, Oort cloud models must invoke an ad hoc assumption that the GRB progenitor distance has a sharp cutoff at between 100 and 500 AU (e.g., Horack et al. 1994). Future instruments capable of more accurate GRB localization (e.g., BeppoSAX and HETE-2) may increase the distance limit. For example, a burst localized with arcminute accuracy could (when compared to an IPN annulus) raise the distance lower limit to thousands of AU.

The Galactic dipole and quadrupole moments of COMPTEL burst locations independently confirm the long-known result that strong bursts are distributed isotropically (Atteia et al. 1987; Hartmann & Epstein 1989). In addition, the COMPTEL measurements mean that GRBs with predominantly hard spectra are probably from the same angular source distribution as the bulk of events observed by BATSE, even though the radial distribution of soft and hard events measured with BATSE intensities may differ (e.g., Belli 1995; Kouveliotou et al. 1996). These results are important in the context of Galactic halo scenarios, in which one expects all the nearer, brighter bursts to exhibit a significant positive dipole moment because of the 8.5 kpc offset of the Sun from the Galactic center. Unfortunately, the absence of a dipole in the COMPTEL bursts is not constraining, owing to the large uncertainties involved.

In the cosmological distance regime, the absence of significant small-angle correlations among the COMPTEL locations is important, since it bears upon the question of burst repetition. Given that the larger 4 yr sample of bursts does not show any significant evidence for small-scale clustering, we must conclude either that the two-burst overlap between GRB 930704 and GRB 940301 was a statistical fluke, or that the two bursts were from a rare repeating source (or source cluster) whose rate of repetition at the COMPTEL sensitivity level is low. If the latter case is true, the lack of excess BATSE bursts from the GRB 930704/GRB 940301 region indicates that the repetition rate from this source is also low at the BATSE sensitivity level. The rarity of repeating GRB sources can be estimated from the COMPTEL observations, where the fraction of observed repeating burst sources must be less than $2/29 = 7\%$. We can obtain this number without the use of the complicated statistical tests that are required in the analysis of BATSE locations (see, e.g., Meegan et al. 1995; Tegmark et al. 1996), since any other possible repeater candidates would be immediately obvious given the small number of COMPTEL bursts and the accuracy of the locations. It is interesting that limits on the fraction of repeating burst sources obtained with BATSE (incorporating thousands of bursts) are about the same as the 7% given here, even though BATSE detects bursts that are an order of magnitude weaker (Meegan et al. 1996; Tegmark et al. 1996). It thus appears that either (1) repeating burst sources are rare, (2) the typical repetition timescale is $\gtrsim 1$ yr, or (3) repeated bursts are too weak to be reliably detected, even by BATSE. More constraining results will come from continued observations and from future instruments with improved location accuracy.

Of further importance in the cosmological distance regime is the lack of significant correlation between COMPTEL bursts and either ACO galaxy clusters or radio-quiet quasars. These findings question the reality of the BATSE/ACO/VCV associations that have been suggested. According to Marani et al. (1997), the strongest cross-correlation signal for BATSE/ACO clusters (~ 3.5–4 σ significance) is obtained for the 27 BATSE 3B bursts with the smallest location errors, and the signal weakens as bursts with larger location errors are included. This could indicate that bright (or high-fluence) bursts are more highly correlated with ACO galaxy clusters than weak events, since bright bursts tend to yield smaller statistical location errors than weaker bursts. This behavior is exactly what we would expect of cosmological GRBs, where only the closest, brightest events would be correlated with relatively nearby ACO galaxies. However, the same correlation should exist in the COMPTEL bursts, since they are the same average brightness and fluence as the 27 well-localized BATSE 3B events. In fact, the two samples share six bursts in common. The only significant difference between the COMPTEL and BATSE burst samples is that the COMPTEL events have harder spectra, on average, than the BATSE bursts. It is possible that hard events are not as strongly correlated with ACO galaxy clusters as are soft bursts, but it is more likely that the BATSE/ACO correlation is a statistical fluke. This conclusion is supported by Hurley et al. (1997), who find that a majority of the ACO clusters that are correlated with BATSE locations are inconsistent with IPN timing annuli, implying that the BATSE/ACO correlation is statistical in origin. The lack of a correlation between COMPTEL burst locations and VCV radio-quiet quasars is less meaningful, since the number of COMPTEL bursts is much smaller than the number of BATSE events (80 bursts with location errors $< 1\overset{\circ}{.}7$) used by Schartel et al. (1997). The weak GRB/quasar correlation using the more numerous BATSE locations may be below the sensitivity of the COMPTEL sample as a result of its larger statistical uncertainty.

While the collective analysis of COMPTEL burst locations offers some insight into the GRB mystery, perhaps the greatest value of the locations is in facilitating rapid counterpart search efforts. The recent discovery of X-ray and optical emission fading on a timescale of hours or days from the BeppoSAX locations of GRB 970228 and GRB 970508 (Costa et al. 1997a, 1997b; van Paradijs et al. 1997; Bond 1997) highlights the value of rapid follow-up studies

using accurate burst locations. During the course of the *CGRO* mission, we have developed a rapid-response system to quickly compute COMPTEL GRB locations and distribute them to multiwavelength observers (primarily optical and radio) around the world (Kippen et al. 1993b). The advantage of using the relatively accurate COMPTEL locations is that they allow deeper searches to be made than previous, and many other current, efforts. The system has been used for several bursts, resulting in some of the most sensitive radio/optical observations of burst locations ever obtained within several hours (see, e.g., Harrison et al. 1995b; McNamara et al. 1996 and references therein). While no fading counterparts have been detected as a result of the COMPTEL rapid-response effort, the observations obtained point the way for future studies, which must concentrate on deep exposures within minutes of a GRB. This is the goal of continuing COMPTEL rapid-response efforts, as well as several ongoing and planned new missions. If the optical light curves of GRB 970228 and GRB 970508 are typical, then wide-field instruments guided by a COMPTEL GRB location within ~ 1 hr may detect the fading counterpart.

We thank C. Meegan and the BATSE operations team for timely communication of BATSE trigger information and N. Schartel for providing his selected quasar catalogs. This research was supported, in part, through the *CGRO* guest investigator program under grant NAG 5-2350. The COMPTEL project is supported by NASA under contract NAS 5-26645, by the Deutsche Agentur für Raumfahrtangelegenheiten (DARA) under grant 50 QV90968, and by the Netherlands Organization for Scientific Research (NWO). D. H. H. acknowledges NASA support under grant NAGW 5-1578, and K. H. is grateful for support under JPL Contract 958056 for *Ulysses* operations, and NAG 5-1560 for the Interplanetary Network. This research made use of data obtained electronically from the High Energy Astrophysics Science Archive Research Center (HEASARC) and from the Astronomical Data Center (ADC).

REFERENCES

Abell, G. O., Corwin, H. G., & Olowin, R. P. 1989, ApJS, 70, 1 (ACO)
Atteia, J.-L., et al. 1987, ApJS, 64, 305
Belli, B. M. 1995, Ap&SS, 231, 43
Bennett, K., et al. 1993, IAU Circ. 5749
Bickert, K. F., & Greiner, J. 1993, in AIP Conf. Proc. 280, Compton Gamma Ray Observatory, ed. M. Friedlander, N. Gehrels, & D. J. Macomb (New York: AIP), 1059
Bond, H. E. 1997, IAU Circ. 6654
Brainerd, J. J. 1996, ApJ, 473, 974
Brainerd, J. J., et al. 1995, ApJ, 441, L39
Briggs, M. S. 1993, ApJ, 407, 126
Briggs, M. S., et al. 1996, ApJ, 459, 40
Clarke, T. E., Blaes, O., & Tremaine, S. 1994, AJ, 107, 1873
Connors, A., et al. 1993a, A&AS, 97, 75
———. 1993b, Adv. Space Res., 13(12), 715
Costa, E., et al. 1997a, IAU Circ. 6576
———. 1997b, IAU Circ. 6649
Dasgupta, A. K. 1979, Ap&SS, 63, 517
de Boer, D. R., et al. 1991, in Data Analysis in Astronomy IV, ed. V. Di Gesù et al. (New York: Plenum), 241
Dermer, C. D. 1996, in AIP Conf. Proc. 384, Gamma-Ray Bursts, ed. C. Kouveliotou, M. S. Briggs, & G. J. Fishman (New York: AIP), 744
Fenimore, E. E., et al. 1993, Nature, 366, 40
Fishman, G. J., et al. 1989, in Proc. of the Gamma Ray Observatory Science Workshop, ed. W. N. Johnson (Greenbelt: NASA/GSFC), 39
Graziani, C., & Lamb, D. Q. 1996, in AIP Conf. Proc. 384, Gamma-Ray Bursts, ed. C. Kouveliotou, M. S. Briggs, & G. J. Fishman (New York: AIP), 382
Greiner, J., et al. 1995, A&A, 302, 121
Grindlay, J. E., & Fazio, G. G. 1974, ApJ, 187, L93
Hanlon, L. O., et al. 1994, A&A, 285, 161
———. 1995, A&A, 296, L41
Harrison, T. E., Webber, W. R., & McNamara, B. J. 1995a, AJ, 110, 2216
Harrison, T. E., et al. 1995b, A&A, 297, 465
Hartmann, D. H., & Blumenthal, G. R. 1989, ApJ, 342, 521
Hartmann, D. H., & Epstein, R. I. 1989, ApJ, 346, 960
Hartmann, D. H., Linder, E. V., & Blumenthal, G. R. 1991, ApJ, 367, 186
Higdon, J. C., & Lingenfelter, R. E. 1990, ARA&A, 28, 401
Horack, J. M., et al. 1994, ApJ, 429, 319
Howard, S., et al. 1993, in AIP Conf. Proc. 280, Compton Gamma Ray Observatory, ed. M. Friedlander, N. Gehrels, & D. J. Macomb (New York: AIP), 793
Hurley, K. 1982, in AIP Conf. Proc. 77, Gamma-Ray Transients and Related Astrophysical Phenomena, ed. R. E. Lingenfelter, H. S. Hudson, & D. M. Worrall (New York: AIP), 85
———. 1986, in AIP Conf. Proc. 141, Gamma-Ray Bursts, ed. E. P. Liang & V. Petrosian (New York: AIP), 1
Hurley, K., et al. 1992, A&AS, 92, 401
———. 1996, in AIP Conf. Proc. 384, Gamma-Ray Bursts, ed. C. Kouveliotou, M. S. Briggs, & G. J. Fishman (New York: AIP), 422
———. 1997, ApJ, 479, L113
Katz, J. I. 1993, in AIP Conf. Proc. 280, Compton Gamma Ray Observatory, ed. M. Friedlander, N. Gehrels, & D. J. Macomb (New York: AIP), 1090
Kippen, R. M., et al. 1993a, in Proc. 23d Intl. Cosmic Ray Conf. (Canada), 1, 85
Kippen, R. M., et al. 1993b, in AIP Conf. Proc. 280, Compton Gamma Ray Observatory, ed. M. Friedlander, N. Gehrels, & D. J. Macomb (New York: AIP), 823
———. 1994a, IAU Circ. 5937
———. 1994b, IAU Circ. 5943
———. 1994c, in AIP Conf. Proc. 307, Gamma-Ray Bursts, ed. G. J. Fishman, J. J. Brainerd, & K. Hurley (New York: AIP), 418
———. 1995a, Adv. Space Res., 15(5), 139
———. 1995b, A&A, 293, L5
———. 1995c, Ap&SS, 231, 231
———. 1995d, Ann. N.Y. Acad. Sci., 759, 425
———. 1995e, in Proc. 24th Intl. Cosmic Ray Conf. (Italy), 2, 61
———. 1996a, in AIP Conf. Proc. 384, Gamma-Ray Bursts, ed. C. Kouveliotou, M. S. Briggs, & G. J. Fishman (New York: AIP), 197
———. 1996b, in AIP Conf. Proc. 384, Gamma-Ray Bursts, ed. C. Kouveliotou, M. S. Briggs, & G. J. Fishman (New York: AIP), 436
———. 1997, Adv. Space Res., in press
Kolatt, T., & Piran, T. 1996, ApJ, 467, L41
Kouveliotou, C., et al. 1996, in AIP Conf. Proc. 384, Gamma-Ray Bursts, ed. C. Kouveliotou, M. S. Briggs, & G. J. Fishman (New York: AIP), 42
Mallozzi, R. S., et al. 1993, in AIP Conf. Proc. 280, Compton Gamma Ray Observatory, ed. M. Friedlander, N. Gehrels, & D. J. Macomb (New York: AIP), 1122
Maoz, E. 1993, ApJ, 414, 877
Marani, G. F., Nemiroff, R. J., Norris, J. P., & Bonnell, J. T. 1997, ApJ, 474, 576
McNamara, B. J., Harrison, T. E., & Williams, C. 1995, ApJ, 452, L25
McNamara, B. J., et al. 1996, ApJS, 103, 173
Meegan, C. A., et al. 1992, Nature, 355, 143
———. 1995, ApJ, 446, L15
———. 1996, ApJS, 106, 65
Mészáros, P., & Rees, M. J. 1992, ApJ, 397, 570
Narayan, R., Paczyński, B., & Piran, T. 1992, ApJ, 395, L83
Nemiroff, R. J., Marani, G. F., & Cebral, J. R. 1994, in AIP Conf. Proc. 307, Gamma-Ray Bursts, ed. G. J. Fishman, J. J. Brainerd, & K. Hurley (New York: AIP), 137
Paczyński, B. 1990, ApJ, 348, 485
Pendleton, G. N., et al. 1996, ApJ, 464, 606
Quashnock, J., & Lamb, D. Q. 1993, MNRAS, 265, 59p
Ryan, J., Kippen, M., & Varendorff, M. 1993, IAU Circ. 5702
Ryan, J. M., et al. 1994a, IAU Circ. 5950
———. 1994b, ApJ, 422, L67
Schaefer, B. E., & Cline, T. L. 1985, ApJ, 289, 490
Schartel, N., Andernach, H., & Greiner, J. 1997, A&A, in press
Schönfelder, V., et al. 1991, IAU Circ. 5369
———. 1993, ApJS, 86, 629
Stacy, G. J., et al. 1996, A&AS, 120, 691
Tegmark, M., et al. 1996, ApJ, 466, 757
van Paradijs, J., et al. 1997, Nature, 386, 686
Varendorff, M. G., et al. 1992, in AIP Conf. Proc. 265, Gamma-Ray Bursts, ed. W. S. Paciesas & G. J. Fishman (New York: AIP), 77
———. 1993, in Proc. 23d Intl. Cosmic Ray Conf. (Canada), 1, 81
Véron-Cetty, M. P., & Véron, P. 1996, A Catalog of Quasars and Active Galactic Nuclei (7th ed.; Garching bei Munchen: ESO), 1
Vrba, F. J. 1996, in AIP Conf. Proc. 384, Gamma-Ray Bursts, ed. C. Kouveliotou, M. S. Briggs, & G. J. Fishman (New York: AIP), 565

Wang, V. C., & Lingenfelter, R. E. 1993, ApJ, 416, L13
Webber, W. R., et al. 1995, AJ, 110, 733
White, R. S. 1993, Ap&SS, 208, 301
———. 1994, in AIP Conf. Proc. 307, Gamma-Ray Bursts, ed. G. J. Fishman, J. J. Brainerd, & K. Hurley (New York: AIP), 620
Winkler, C., et al. 1986, Adv. Space Res., 6(4), 113
Winkler, C., et al. 1992a, A&A, 255, L9
———. 1992b, in AIP Conf. Proc. 265, Gamma-Ray Bursts, ed. W. S. Paciesas & G. J. Fishman (New York: AIP), 22
———. 1993, in AIP Conf. Proc. 280, Compton Gamma Ray Observatory, ed. M. Friedlander, N. Gehrels, & D. J. Macomb (New York: AIP), 845
———. 1995, A&A, 302, 765